

# Unexpected Weak Spatial Variation of Local Density of States Induced by Individual Co Impurity Atoms in $\text{Na}(\text{Fe}_{1-x}\text{Co}_x)\text{As}$ Revealed by Scanning Tunneling Spectroscopy

Huan Yang<sup>1</sup>, Zhenyu Wang<sup>2</sup>, Delong Fang<sup>1</sup>, Sheng Li<sup>1</sup>, Toshikazu Kariyado<sup>3</sup>, Genfu Chen<sup>2</sup>, Masao Ogata<sup>3</sup>, Tanmoy Das<sup>4</sup> and A. V. Balatsky<sup>4</sup> and Hai-Hu Wen<sup>1,\*</sup>

<sup>1</sup>Center for Superconducting Physics and Materials,

National Laboratory of Solid State Microstructures and Department of Physics, Nanjing University, Nanjing 210093, China

<sup>2</sup>National Laboratory for Superconductivity, Institute of Physics and National Laboratory for Condensed Matter Physics, Chinese Academy of Sciences, Beijing 100190, China

<sup>3</sup>Department of Physics, University of Tokyo, 7-3-1 Hongo, Bunkyo,

Tokyo 113-0033 and JST, TRIP, Sanbancho, Chiyoda, Tokyo 102-0075, Japan and

<sup>4</sup>Theoretical Division and Center for Integrated Nanotechnologies, Los Alamos National Laboratory, Los Alamos, NM, 87545, USA

We use spatially resolved scanning tunneling spectroscopy in  $\text{Na}(\text{Fe}_{1-x}\text{Co}_x)\text{As}$  to investigate the impurity effect induced by Co dopants. The Co impurities are successfully identified, and the spatial distributions of local density of state at different energies around these impurities are investigated. It is found that the spectrum shows negligible spatial variation at different positions near the Co impurity, although there is a continuum of the in-gap states which lifts the zero-bias conductance to a finite value. Our results put constraints on the  $S\pm$  and  $S++$  models and sharpen the debate on the role of scattering potentials induced by the Co dopants.

PACS numbers: 74.55.+v, 74.62.Dh, 74.20.Rp, 74.70.Xa

## I. INTRODUCTION

According to the Anderson's theorem<sup>1,2</sup>, the Cooper pairs with singlet pairing can survive in the presence of non-magnetic impurities, while the magnetic impurities are detrimental to superconductivity yielding a unique pattern of the electronic local density of states (LDOS). This view has been well established in the conventional superconductors<sup>3</sup>. In superconductors with gap nodes, even the nonmagnetic impurities can be strong pair breakers<sup>2,4</sup>. In the iron-based superconductors<sup>5</sup>, the pairing mechanism remains as a hot and unresolved issue. It is proposed that the pairing is mediated by the antiferromagnetic (AF) spin fluctuations resulting in a  $S\pm$  pairing<sup>6,7</sup>, which now becomes a widely perceived picture. The experimental evidence that directly supports  $S\pm$  pairing is still quite rare. One was drawn from the scanning tunnelling spectroscopy (STS) and the quasi-particle interference measurements in  $\text{Fe}(\text{Se},\text{Te})$ <sup>8</sup>. Another indirect evidence is the observation of the resonance peak of the imaginary part of the spin susceptibility at  $(\pi, \pi)$  in the inelastic neutron scattering experiment<sup>9</sup>. Theoretically it was argued that this type of pairing should also be fragile to the non-magnetic impurities<sup>10-12</sup>. One of the puzzles concerning this model is why superconductivity survives up to a relatively high temperature in some doped samples, such as the  $\text{Ba}(\text{Fe}_{1-x}\text{Te}_x)_2\text{As}_2$  ( $T=\text{Co}, \text{Ni}, \text{Ru}, \text{etc.}$ ), where the dopants are supposed to be the pair breakers. The spatial and energy dependent LDOS induced by the impurity scattering can be regarded as the *fingerprints* for a formal check on this peculiar pairing model<sup>10-15</sup> which can be measured by the STS. After cleaving an iron-based superconductor, one usually encounters a polar and messy surface<sup>16,17</sup>, while an atom-

ically resolved image was sometimes observed in a reconstructed surface<sup>18-20</sup>. However, it is very difficult to locate a *well-defined quantum impurity* and investigate the related LDOS on such surfaces with an exception in  $\text{Ca}(\text{Fe}_{1-x}\text{Co}_x)_2\text{As}_2$ <sup>20</sup>. In this paper, we report the success in locating the Co impurities and measuring the spatially resolved STS at different energies and temperatures obtained from the  $\text{Na}(\text{Fe}_{1-x}\text{Co}_x)\text{As}$  single crystals. Our results indicate an unexpected weak variation of the STS and LDOS when going through a Co impurity site. Combined with the theoretical calculations, we propose explanations for this dichotomy (finite LDOS but weak variation). Our findings put constraints on the theoretical models of the pairing state.

## II. EXPERIMENTS

High quality  $\text{Na}(\text{Fe}_{1-x}\text{Co}_x)\text{As}$  single crystals were synthesized by the flux method<sup>21</sup>. The samples were cleaved at room temperature in an ultra-high vacuum with a base pressure better than  $2 \times 10^{-10}$  Torr, then transferred into the scanning tunneling microscopy (STM) head immediately and cooled to a desired temperature. The STS were measured with an ultra-high vacuum, low temperature and high magnetic field scanning probe microscope USM-1300 (Unisoku Co., Ltd.). In all STM/STS measurements, Pt/Ir tips were used. The surface topographies were recorded using a bias voltage of  $V_{\text{bias}} = 40$  mV and tunneling current of  $I_t = 100$  pA. To reduce the noise of the differential conductance spectra, a lock-in technique with an ac modulation of 0.1 mV at 987.5 Hz was typically used.

### III. RESULTS

#### A. Sample characterization

Figure 1(a) shows the temperature dependence of the volume dc magnetization ( $M$ ) after zero-field-cooling (ZFC) and field cooling (FC) processes. The magnetization on the samples of two doping levels showed sharp superconducting transitions with  $T_c \approx 16.8$  K for  $x = 0.05$  and  $T_c \approx 21.2$  K for  $x = 0.025$ . Since the single crystals are thin and plate like, the demagnetizing factor is relatively large; that is the reason the ZFC magnetization values of these two samples are different. The error in the measurement of dimensions, especially the thickness, could give some error in the calculation of the ZFC susceptibility. Figure 1(b) shows the resistive transitions of the two samples. It is clear that the sample with more charge doping level ( $x=0.05$ ) is lower than that at the optimal doping ( $x=0.025$ ) although their  $T_c$  values are opposite. The different values of the resistivity at 300 K may be related to the charge doping effect in the samples.

#### B. Identification of Co dopant atoms in $\text{Na}(\text{Fe}_{1-x}\text{Co}_x)\text{As}$

Figures 2(a) and 2(b) present the topographic image of the cleaved surface of samples with (a)  $x = 0.025$  and (b)  $x = 0.05$ . The background shows a well-ordered square lattice with a constant of  $3.80 \text{ \AA}$ . Because the Na atoms are distributed equally into two layers between two neighboring As-layers, the cleaving occurs between the two Na layers leading to an un-polar (charge neutral) surface<sup>22</sup>. In both samples, beside the observed square lattice, one can see some rectangular blocks with two unit cells constructed by six Na atoms (hereafter named a  $2 \times 1$  block) which are a bit brighter than the background as shown in Figs. 2(a) and 2(b). These blocks align along either  $[100]$  or  $[010]$  directions. The brightness is enhanced when many blocks overlap each other [marked by an arrow in Fig. 2(a)]. After considering the arrangement of Na atoms in one  $2 \times 1$  block, we argue that each block is corresponding to one individual Co impurity atom. Two reasons can be given to support this argument, as addressed below.

Firstly, when one Co atom is doped to the Fe site, it naturally neighbors with six Na atoms on the surface layer, forming a 2-unit-cell rectangular ( $2 \times 1$ ) block as illustrated by Fig. 2(e), the orientation of the  $2 \times 1$  block is determined by the selective positioning of the Co atom on the  $a$ -axis or  $b$ -axis of the Fe-As square lattice. Secondly, counting the ratio between the number of the typical  $2 \times 1$  blocks and the total number of Fe and Co atoms, we find that it is very close to the doped concentration of Co, i.e., the nominal value of  $\text{Co}/(\text{Fe}+\text{Co})$  in the samples. We counted the number of  $2 \times 1$  blocks as shown in Fig. 2(f) and (g). The very bright regions on the over-doped  $\text{Na}(\text{Fe}_{0.95}\text{Co}_{0.05})\text{As}$

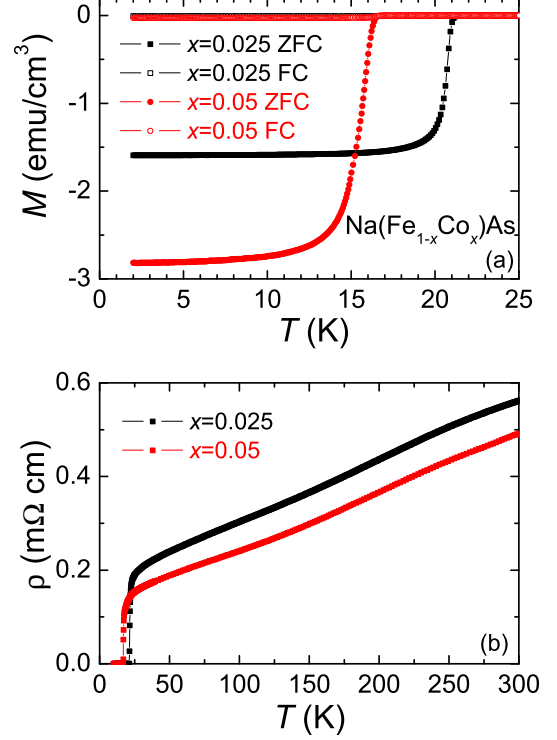


FIG. 1: (Color online) (a) Temperature dependence of volume magnetization of  $\text{Na}(\text{Fe}_{0.975}\text{Co}_{0.025})\text{As}$  and  $\text{Na}(\text{Fe}_{0.95}\text{Co}_{0.05})\text{As}$  single crystals after zero-field cooling (ZFC) and field cooling (FC) at 10 Oe. The difference in the ZFC magnetization of the two samples comes from the different demagnetizing effect. (b) Temperature dependence of resistivity for the two  $\text{Na}(\text{Fe}_{1-x}\text{Co}_x)\text{As}$  samples with different doping levels.

sample are originated from overlapping of several  $2 \times 1$  blocks which can be distinguished from the differential figure as shown in Fig. 2(h). The stacking blocks are distinguished from different height of the Na atoms and contrast level of the experimental image. The quantities of Co atoms counted on  $\text{Na}(\text{Fe}_{0.975}\text{Co}_{0.025})\text{As}$  and  $\text{Na}(\text{Fe}_{0.95}\text{Co}_{0.05})\text{As}$  samples are 64 and 110 respectively with the counting error of 10%, while the total number of Fe sites should be 2677 in such  $14 \text{ nm} \times 14 \text{ nm}$  area. Only one bright region with the question mark at the bottom edge on the  $\text{Na}(\text{Fe}_{0.95}\text{Co}_{0.05})\text{As}$  sample as shown in Fig. 2(g) hasn't been taken into account, due to the uncertainty. The corresponding ratio of doped Co atoms over all the Fe+Co sites  $\text{Co}/(\text{Fe}+\text{Co})$  on the sample with  $x = 0.025 \approx 2.39 \pm 0.24 \%$ ; while on the sample  $x = 0.05$ , we get  $\text{Co}/(\text{Fe}+\text{Co}) \approx 4.11 \pm 0.41 \%$ . The two calculated ratios are comparable with their chemical doping levels 2.5% and 5%, respectively. This could not be achieved by accident. We also checked the height where several blocks overlap each other. As shown in Figs. 3 (a), (b),

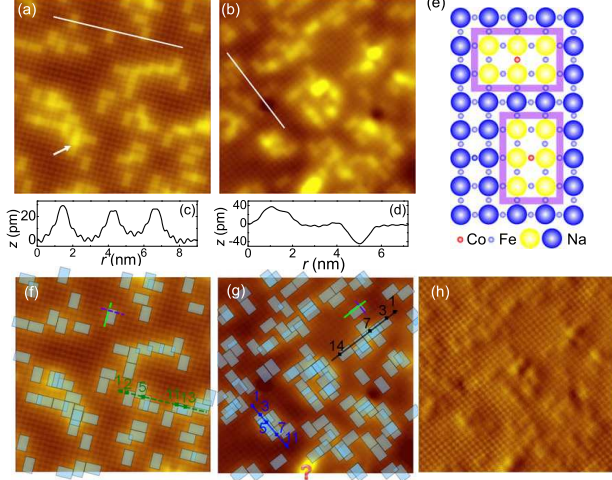


FIG. 2: (Color online) (a, b) High-resolution topography in a region of  $14 \times 14 \text{ nm}^2$  on  $\text{Na}(\text{Fe}_{1-x}\text{Co}_x)\text{As}$  samples with  $x = 0.025$  (a) and  $x = 0.05$  (b). (c, d) The spatial dependence of height  $z$  measured along the white lines marked in (a) and (b). (e) Illustration for atoms near the Co-impurity sites. It is clear that each Co atom neighbors with six Na atoms (highlighted by the yellow circles), forming the  $2 \times 1$  rectangular block (see text). (f, g) Illustration for counting the  $2 \times 1$  blocks on (a, b), and the  $2 \times 1$  block patterns are marked with light-blue rectangles. (h) The differential picture of (b) which is helpful to make the counting.

(d), and (e), we present the height distributions crossing one single  $2 \times 1$  block in two perpendicular directions. We used these distributions as basic cells to simulate the height where several blocks overlap by a simple summation. The simulation is undertaken based on the distribution of the  $2 \times 1$  blocks shown in Fig. 2(f) and (g). The accumulated height equals to the summation of the total contributions given by several blocks demonstrated by the frames. We test this simple method along three typical lines in Fig. 2(f) and (g). One can see that the consistency between the simulated results and the data is remarkable. This clearly convinces that the very bright spots are constructed by several  $2 \times 1$  blocks overlapping each other, which validates the counting method we proposed here. This result may also suggest that the local work function on six Na atoms of the  $2 \times 1$  blocks is reduced, which results in a linear enhancement of the height when the blocks overlap each other. Such conclusion can be derived by the expression of tunneling current if the second order small quantities in the Taylor expansion are omitted.

Recently, Erwin and Mazin have performed first principles calculations of the map of tunnelling current in  $\text{NaFeAs}$  with an isolated surface Co impurity<sup>23</sup>, and found that the calculated topographic image closely resembles ours and reproduces the  $2 \times 1$  block that we assigned to a Co impurity. These  $2 \times 1$  blocks seem to

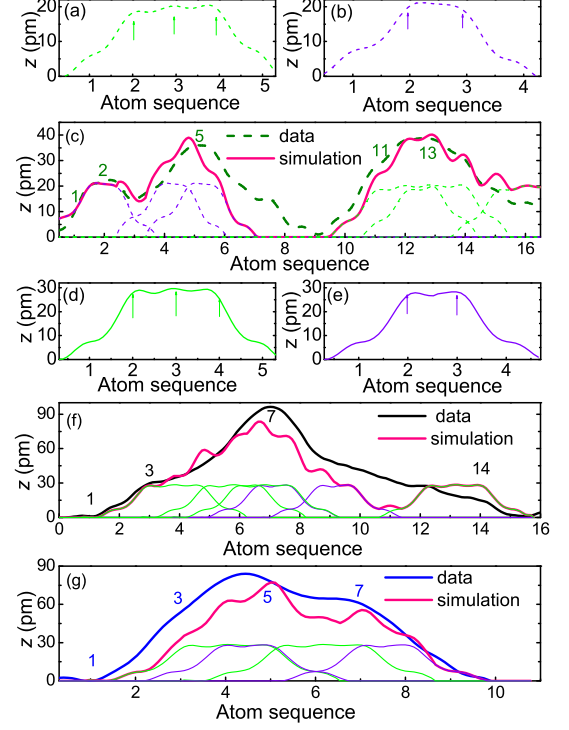


FIG. 3: (Color online) Simulations of the height on overlapping of  $2 \times 1$  blocks. (a),(b),(d) and (e) are line profiles of a single block marked by green and violet dashed/solid lines in Figs. 2(f) and (g), while (c), (f) and (g) show three simulated line profiles of combined altitude by overlapping blocks illustrating in Figs. 2(f) and (g). One can find that the simulated lines match well with the experimental data.

be slightly higher (about 30 pm) than the surrounding atoms, as shown by the line-cut in Figs. 2(a) and (b) with the landscape shown in Figs. 2(c) and (d), respectively. At some positions, we see dark areas characterized by a lower height, as shown by the line-cut in Figs. 2(b) and (d). These are probably induced by the vacancies of the atoms beneath the surface layer.

### C. Impurity state on Co-dopant site

#### 1. STS far away from the Co-impurity

In the sample with  $x = 0.05$  we measured the evolution of tunnelling spectrum with temperature and showed it in Fig. 4(a). At low temperatures, two coherent peaks near the gap edges can be clearly seen. The asymmetric structure of the STS curve is induced by the background, which can be evidenced by the data measured at 25 K ( $> T_c = 16.8 \text{ K}$ ) as shown in Fig. 3(b). In Fig. 4(c), we present the experimental STS at 1.7 K that normalized by the data at 25 K. On the STS curve, there is a finite value of zero-bias conductance, which seems to

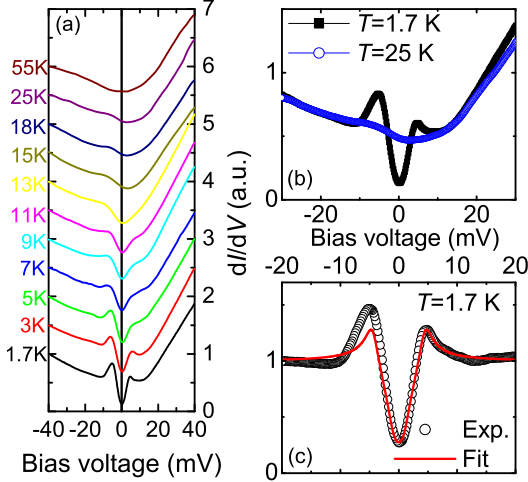


FIG. 4: (Color online) (a) The STS measured on  $\text{Na}(\text{Fe}_{0.95}\text{Co}_{0.05})\text{As}$  at a position far away from the Co-impurities at temperatures from 1.7 K to 55 K. (b) STS taken at 1.7 K and 25 K. (c) The STS measured at 1.7 K normalized by that of 25 K (symbols). The solid line is a fit according to the Dynes formula with a gap of 4.5 meV and a scattering rate of  $\Gamma = 0.7$  meV.

be a common feature of Co-doped samples<sup>24–26</sup>, and will be addressed later. No feature of two gaps is observed here. This is consistent with the angle-resolved photo-emission spectroscopy measurements on the same sample, which indicates the same gaps,  $\sim 5$  meV, on both the electron and hole pockets.<sup>27</sup> The normalized data was fitted with the Dynes model<sup>28</sup> with the gap function  $\Delta(\theta) = \Delta[(1-a)\cos 2\theta + a]$  to fit the experimental data. First we try the isotropic S-wave with anisotropy factor  $a = 1$ , as shown in the Fig. 5(a). The result is shown by the green curve. In Fig. 5(b), we show the fitting curves with different anisotropy  $a$  and  $\Gamma$ . It is found that an optimized fitting can be obtained when using  $a = 0.65$ , i.e.,  $\Delta(\theta) = 4.5(0.35\cos 2\theta + 0.65)$  meV and scattering rate  $\Gamma = 0.7$  meV. One point we should mention is that, there is a slight enhancement of  $dI/dV$  at about -5 meV even above  $T_c$ , e.g., at 25 K. This feature is smeared out at elevated temperatures and vanishes at about 55 K. Interestingly this feature seems to be linked with the asymmetry of the STS, for example, the coherence peak at  $-\Delta = -4.5$  meV is higher than that at  $+\Delta = 4.5$  meV, even at 1.7 K. The relationship between the high temperature feature and the asymmetric superconducting coherence peaks remains to be understood.

## 2. STS across a Co-impurity

In order to have a detailed comparison between the LDOS patterns as expected by the theoretical models and

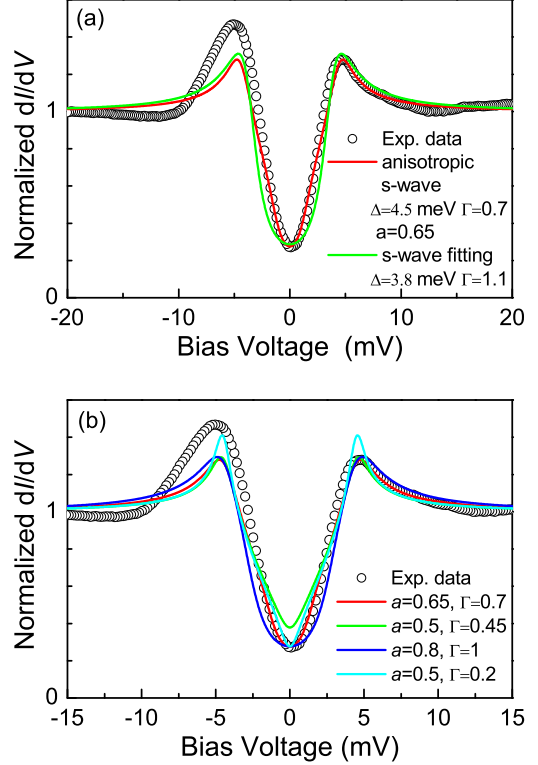


FIG. 5: (Color online) STS measured on  $\text{Na}(\text{Fe}_{0.95}\text{Co}_{0.05})\text{As}$  at 1.7 K and the fitting with different gap functions (a) and different values of fitting parameters for anisotropic s-wave gaps (b).

that induced by the Co-impurity, we select a  $2 \times 1$  block and do the spatial resolved STS measurements with spacing of every half lattice constant, as marked by the dots in Fig. 6(a). The raw data of STS are shown in Figs. 6(b) and 6(c) for the two perpendicular directions. The data measured right on top of the Co-impurity is shown here by a red curve. It is astonishing that the shape of the STS does not change in any noticeable way upon moving through the Co-impurity. The value of  $dI/dV$  taken from these STS curves at three typical voltages ( $V_{\text{bias}} = -4.3, 0$ , and  $4.3$  mV) are shown in Figs. 6(d) and 6(e) with respect to the positions. One can clearly see that the LDOS at either zero energy or the gap edges are quite uniform.

In order to examine the spatial dependence of the spectrum on the Co site and nearby, we show the spectra at different positions in Fig. 7(a) and 7(b). We also measured the STS just on the Co site in a large bias voltage range as shown in Fig. 7(c). One can find an asymmetric background which is similar to the spectra measured on  $\text{LiFeAs}$ <sup>22</sup>. The theoretical simulation indicates that there are clear Co dopant induced resonances at -800 mV and 200 mV in  $\text{BaFe}_2\text{As}_2$ <sup>13</sup>, and some special characteristics



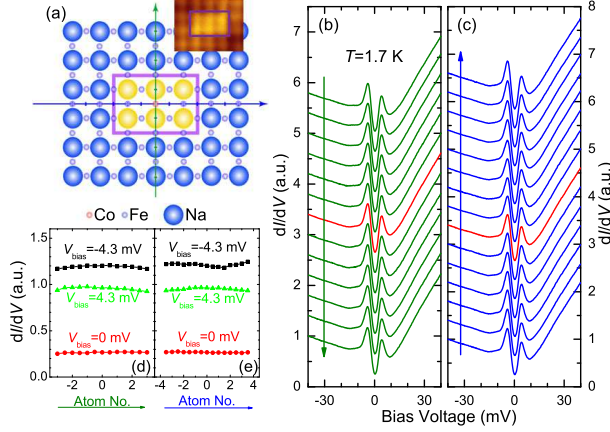


FIG. 6: (Color online) (a) Illustration of the atomic structure based on the topographic image (shown by the inset) of  $\text{Na}(\text{Fe}_{0.95}\text{Co}_{0.05})\text{As}$  at 1.7 K, with a Co-impurity highlighted by a red circle surrounded by Na atoms (big yellow and blue circles). (b, c) Spatially resolved STS measured along the two arrowed lines in (a) with a spacing of every half lattice constant. The red lines show data measured just at the center of the  $2 \times 1$  rectangular block. (d, e) The value of  $dI/dV$  determined near the gap edge ( $-4.3$  meV and  $4.3$  meV) and zero bias when crossing the Co-impurity point.

at about 150 mV was observed and suggested to image Co atoms on the surface of slightly Co-doped  $\text{CaFe}_2\text{As}_2$ <sup>20</sup>. However we didn't find any characteristic features within  $\pm 200$  meV at either the Co site, or somewhere far away from the Co sites. To investigate the spectrum affected by the black holes and the very bright spots originated from the overlapping of several  $2 \times 1$  blocks in Fig. 2(b), we measured the spectra on such places and showed them in Fig. 7(d). One can see that the gap values as well as the bottom heights are almost the same at different positions. The superconducting coherence peaks on the spectrum measured on a bright spot are suppressed comparing to the one measured at the point without any features. The black holes seem to affect the spectrum very little which suggests that it arises from the depletion of some Na atoms on the top surface.

### 3. Theoretical simulated results of the LDOS on the Co site

In order to understand the spatial dependence of the spectrum on the Co site and nearby in our experiments, we did theoretically calculations based on the  $S\pm$  and  $S++$  models. First we analyze the gap functions of the  $S\pm$  wave superconductivity obtained in random phase approximation (RPA). We use the multi-orbital Hubbard model proposed by Kuroki et al.<sup>7</sup>, which is down-folded from the first-principle calculation. In this scheme, five Fe 3d orbitals of  $d_{3z^2-r^2}$ ,  $d_{zx}$ ,  $d_{yz}$ ,  $d_{x^2-y^2}$ , and  $d_{xy}$  are

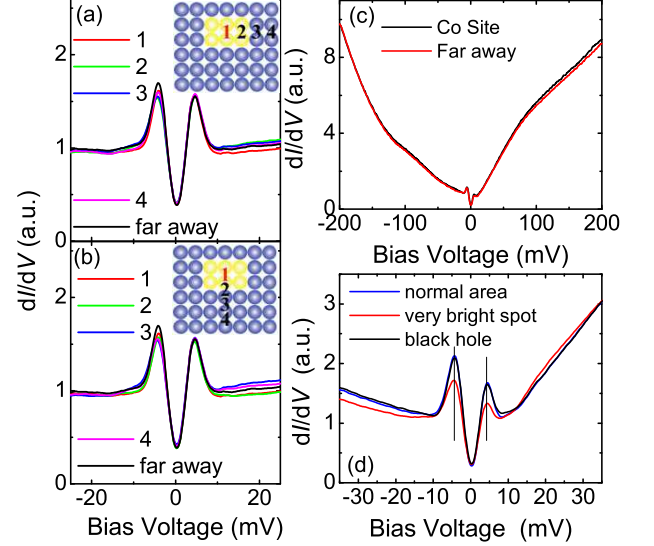


FIG. 7: (Color online) (a, b) The tunnelling spectra normalized by the normal state one measured at different positions: 1, on site of the impurity, 2-4 corresponds to those measured at the 2nd, 3rd and 4th lattice constants away in two perpendicular directions. (c) STS measured on  $\text{Na}(\text{Fe}_{0.95}\text{Co}_{0.05})\text{As}$  at 1.7 K. It is found that the STS measured just on the Co site is very similar to the one measured far away and it has no special feature in the voltage range from  $-200$  mV to  $200$  mV besides the superconducting gap at low energies. An asymmetric background is seen here which may be induced by the multi-band and the band edge effect. (d) STS measured on a very bright spot, a black hole and somewhere far away from such features. One can see that the energy gap values are almost the same at these specific locations.

kept, and the hopping integrals between these orbitals for the  $\text{LaFeAsO}$  (1111) system is used. This will be justified since the Fermi surface for  $\text{NaFeAs}$  near  $k_z = 0$  is similar to that of  $\text{LaFeAsO}$ , although  $\text{NaFeAs}$  has stronger three-dimensionality than 1111 system. The effect of the  $z$ -direction hopping on the impurity scattering is a future problem. In this paper, we do not go into details of the material-dependent model, but instead we compare the experiment and theory in a simple model which contains essence of the multi-band unconventional ( $S\pm$  and  $S++$ ) superconductivity. It is found that, when we use orbital representation instead of band representation, the gap functions obtained in RPA can be reproduced quite well by using the real-space short-range pairings (up to next-nearest-neighbor sites). The details are explained elsewhere.<sup>29</sup> Note that, in the RPA calculation around  $T_c$ , the absolute values of the gap functions are not determined, and only their relative sizes are obtained. Therefore, we adjust the largest gap value to be consistent with the experiment. On the other hand, for the  $S++$  case, the gap functions are obtained from the analysis of the five-orbital attractive Hubbard model.

The impurity is treated as a single site in the two-dimensional square lattice with an on-site impurity potential. The orbital dependence of the potential is neglected. The value of the impurity potential is chosen as  $I = 1.0$  eV<sup>13</sup> and  $I = -0.35$  eV<sup>14</sup> according to the previous first-principle calculations. The gap functions around the impurity site are assumed to be spatially uniform for simplicity. The effect of this simplification is discussed shortly. The actual calculation of LDOS is performed using Chebyshev polynomial expansion method<sup>30</sup> with  $900 \times 900$  lattice sites and 3600 polynomials. The Lorentzian-type broadening kernel is used and the broadening factor is determined so as to make  $\gamma/\Delta_{\text{max}}$  consistent with experiment. Because of this broadening, LDOS at  $E = 0$  remains finite even in the S++ case, which comes mainly from the tail of the peak at the gap edge. The electron number is fixed at  $n = 6.05$  by adjusting the chemical potential.

There are two important factors that should be included when we compare the theoretical calculations with experimental data. First, there is a band renormalization effect due to electron-electron correlation which is neglected in the first-principle calculations. In iron pnictides, the effective mass obtained in ARPES is larger than that obtained in the first-principle calculation by a factor of about 2.5. Therefore, in order to take account of the band renormalization factor (not included in the first-principle calculations), the hopping integrals and site-potentials in the model Hamiltonian should be reduced by a factor 2.5. By considering this effect, we reduce the energy scale of the obtained results by factor 2.5, for simplicity. The other important factor is that the experimental tunneling spectra were taken under the condition of constant tunneling current. In all the experiment measurements, the spectra were taken with the same initial tunneling current (e.g., 100 pA) at some bias voltage  $V_0$  (e.g., 40 mV). So there was a normalization process using the integral area of sample LDOS from 0 to  $V_0$  of each curve if we simply considered the tip LDOS as a constant.<sup>19</sup> Such normalization makes very little change of the tip height which can be omitted because the tunneling current decays exponentially with increasing of height. This means that LDOS obtained theoretically should be normalized in accordance with the experimental condition of constant current. This is carried out by rescaling the amplitude of LDOS for each site so that the energy integral of LDOS between  $E = 0$  to -20 meV becomes a constant for the negative parts of calculations have fewer features.

After these treatments, LDOS shown in Figs. 8(e)-8(g) are obtained. For the case of S $\pm$  and scattering potential  $I = 1.0$  eV [Fig. 8(e)] and at the impurity site, the simulated data indicate a strong in-gap bound state peak at zero energy as shown in the previous paper<sup>11</sup>. For other cases, the bound state peaks are absent and shape of the spectrum changes when it is moving away from the impurity site. From Figs. 8(f) and 8(h), we can see that the results with  $I = -0.35$  eV for S++ (Fig.8(h)) are quite

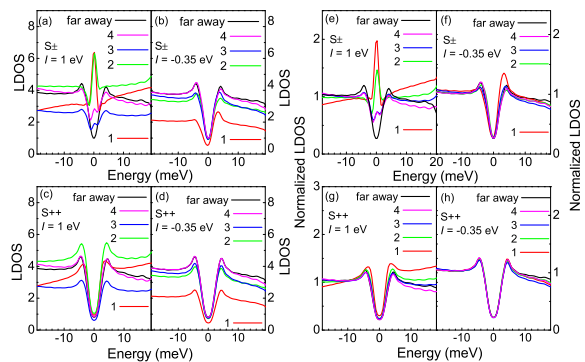


FIG. 8: (Color online) (a-d) Un-normalized STS calculated in a simplified model based on S++ and S $\pm$  pairing gaps at several sites near the impurity with the same spatial registration as the experiment (based on the band parameters of the LaFeAsO system<sup>29</sup>) (e-f) Curves of (a-d) normalized by the integral area of LDOS from -20 mV to 0 mV in corresponding to the constant-current situation in the experiment.

consistent with the experimental data. However, we cannot exclude the possibilities of S $\pm$  model with  $I = -0.35$  eV and the S++ model with  $I = 1$  eV, since the simulated results and experimental data are not very distinct.

At the end of this part, we want to check the validity of neglecting the spatial dependence of the gap functions around the impurity site. For this purpose, we have to determine the gap functions around the impurity self-consistently by solving the Bogoliubov-de Gennes equation iteratively just as in Ref.<sup>11</sup>. However, a large numerical cost of solving Bogoliubov-de Gennes equation limits the accessible energy scale. If we try to reproduce the experimental gap size, the self-consistency calculation becomes unstable or unrealistic suffered from the finite-size effect of the available lattice. This is just a technical reason, but we have to assume large attractive interactions in order to obtain self-consistent solutions. In this calculation, we solve Bogoliubov-de Gennes equation used in Ref.<sup>11</sup> that is constructed so as to reproduce the RPA S $\pm$  results and contains attractive interactions up to the next-nearest-neighbor sites. On the other hand, for the S++ case, we use a model with short-range attractive interaction. We use a lattice with  $28 \times 28$  sites with an impurity at the center in order to obtain eigenvalues and eigenfunctions. For the LDOS calculation, we use the “supercell” method in which  $28 \times 28$ -site lattice with an impurity is treated as a “unit cell” and the whole system is assumed to be composed of a  $13 \times 13$  repeat of this unit cell.<sup>11</sup> Figures 9(a)-9(d) show the LDOS obtained by this self-consistent calculation. Since the attractive interaction is large, the obtained gap function is larger than the experimentally observed gap values. Note that LDOS is not normalized and the band renormalization factor is not taken into account. For comparison, we show the LDOS without self-consistent calculation in Figs 8(a)-8(d), which are identical with Figs. 8(e)-8(h) but they are

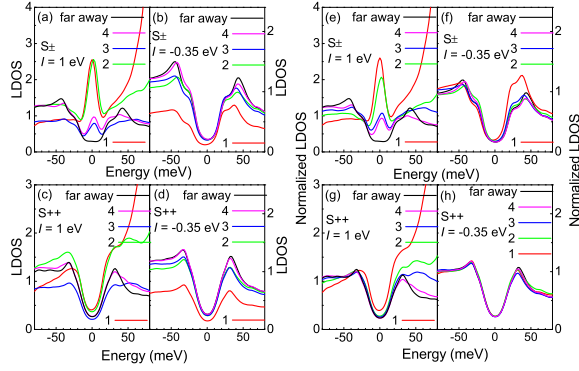


FIG. 9: (Color online) (a-d) The STS calculated in a five-orbital model based on  $S++$  and  $S\pm$  pairing gaps at several sites near the impurity with the same spatial registration as the experiment (based on the band parameters of the  $\text{LaFeAsO}$  system<sup>29</sup>) (e-f) Curves of (a-d) normalized by the integral area of LDOS from -80 mV to 0 mV in corresponding to the constant-current situation in the experiment.

not normalized. From this comparison, we can see that the results do not change qualitatively even if we assume a site-independent gap functions [Figs 8(a)-8(d)] compared with the full self-consistent calculation in Figs.9(a)-9(d). One dominant difference is a rather large peak at  $E > 50$  meV in Figs.9(a) and 9(c) (i.e., for  $I = 1.0$  eV case) on the impurity site (line 1: red curve). We find that this large peak is due to the impurity-induced resonant state that exists even in the normal state. Although the impurity-induced resonant states exist in Figs. 8(a) and 8(c), it is located outside of the energy-range shown here.

#### D. Discussion on the Impurity effect by Co doping

The experimentally measured STS seems to change very weakly when crossing the Co site as mentioned above. On one hand, we don't see the sharp bound state peaks at the impurity site as theoretically predicted for the  $S\pm$  pairing gap for  $I = 1$  eV with the non-magnetic impurities. On the other hand, we do see a continuum of in-gap states, which lifts the zero-bias conductance to a finite value. Theoretically we find that the effect of Co-impurity on LDOS is similar both for  $S\pm$  and  $S++$  case when  $I = -0.35$  eV. One may argue that the scattering effect given by the Co-impurity is very weak i.e.,  $I \sim 0$ . However, specific heat data shows a significant residual specific heat coefficient  $\gamma_0 = 9.8$  mJ/mol·K<sup>2</sup> (as shown in Fig. 10) suggest that the scattering in the Co-doped case is significant. This phenomena occurs in other doped samples as well when the dopants go directly to the Fe sites<sup>31</sup>. The density functional calculation of the local substitution of Co or Ni for Fe suggest that no extra charge carriers are doped into the system<sup>32</sup>. In this case, the Co-impurity should behave as an impurity scatterer

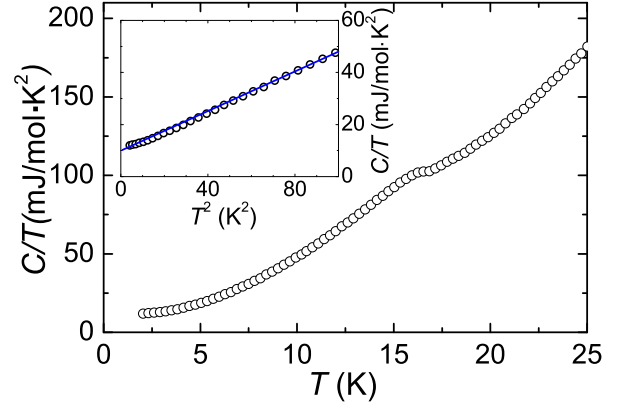


FIG. 10: (Color online) Temperature dependence of specific heat of  $\text{Na}(\text{Fe}_{0.95}\text{Co}_{0.05})\text{As}$ . The inset shows an enlarged view of the same data in the low temperature limit.

for Cooper pairs<sup>33</sup>. Provided the expectable influence given by the Co-impurities, it is paramount that we understand the lack of the spatial variation of the LDOS spectrum nearby the Co-site within the  $S\pm$  model.

Now we discuss the possible reasons for this dichotomy, and constraints given by our results on the theoretical pairing models. Although there is a discrepancy (especially near the gap edge) between the experimental data and the theoretical results, the  $S++$  model would give a much better consistency. However, the  $S\pm$  model may still be relevant in the following circumstances: (1) The scattering potential  $I$  is around -0.35 eV, as shown in Fig. 8(f). In the absence of precise independent assessment on the scattering potential, we assume that the scattering potential is relatively weak. (2) The Co-impurity may behave as an extended scattering center, so that the scattering between the electron and hole Fermi pockets (if would be the cause of pairing) will not be affected due to the finite range. Since the inter pocket scattering is the major cause for the pairing based on the  $S\pm$  model, that may be the reason why the superconductivity survives in the presence of such impurities. With this picture, the obvious scattering as revealed by the residual resistivity and specific heat data are probably induced by the intra-pocket scattering which can suppress the superconductivity moderately, but not strongly. Such scattering results in the expectation of in-gap filled states with no sharp resonance states seen. (3) The last possibility would be that the pairing is induced by strong local super-exchange effect<sup>34,35</sup> which will certainly not be weakened so much by the non-magnetic impurity and relatively weak scattering.

## IV. CONCLUSIONS

In summary, we successfully locate the doped Co atoms in  $\text{Na}(\text{Fe}_{1-x}\text{Co}_x)\text{As}$  using scanning tunnelling microscopy. Negligible spatial variation of the tunnelling spectrum near the Co impurity is observed, which is in sharp contrast with the theoretical simulations with the  $S\pm$  model taking  $I = 1$  eV. We explain our data with the  $S++$  or  $S\pm$  models. The  $S++$  model can be consistent with the data, however, the  $S\pm$  model is still relevant in the following three cases: (1) The scattering potential  $I$  given by a Co dopant is relatively small, for example,  $I \sim 0.35$  eV; (2) The Co-dopants give rise to the extended scattering centers which will not significantly affect the

interpocket scattering; (3) The pairing may be induced by local strong magnetic super-exchange effect.

## Acknowledgments

This work is supported by the Ministry of Science and Technology of China (973 projects: 2011CBA00102, 2012CB821403, 2010CB923002), NSF and PAPD of China. Work at Los Alamos was supported by the U.S. DOE under contract No. DE-AC52-06NA25396 and the Office of Science (BES).

\* hhwen@nju.edu.cn

- 
- <sup>1</sup> P. W. Anderson, J. Phys. Chem. Solids **11**, 26 (1959).
  - <sup>2</sup> A. Balatsky, J. X. Zhu, and I. Vekhter, Rev. Mod. Phys. **78**, 373 (2006).
  - <sup>3</sup> A. Yazdani, B. A. Jones, C. P. Lutz, M. F. Crommie, and D. M. Eigler, Science **275**, 1767 (1997).
  - <sup>4</sup> S. H. Pan, E. W. Hudson, K. M. Lang, H. Eisaki, S. Uchida, and J. C. Davis, Nature **403**, 746 (2000).
  - <sup>5</sup> Y. Kamihara, T. Watanabe, M. Hirano, and H. Hosono, J. Am. Chem. Soc. **130**, 3296 (2008).
  - <sup>6</sup> I. I. Mazin, D. J. Singh, M. D. Johannes, and M. H. Du, Phys. Rev. Lett. **101**, 057003 (2008).
  - <sup>7</sup> K. Kuroki, S. Onari, R. Arita, H. Usui, Y. Tanaka, H. Kontani, and H. Aoki, Phys. Rev. Lett. **101**, 087004 (2008).
  - <sup>8</sup> T. Hanaguri, S. Niitaka, K. Kuroki, and K. Takagi, Science **328**, 474 (2010).
  - <sup>9</sup> A. D. Christianson, E. A. Goremychkin, R. Osborn, S. Rosenkranz, M. D. Lumsden, C. D. Malliakas, I. S. Todorov, H. Claus, D. Y. Chung, M. G. Kanatzidis, R. I. Bewley, and T. Guidi, Nature (London) **456**, 930 (2008).
  - <sup>10</sup> H. Kontani, and S. Onari, Phys. Rev. Lett. **103**, 177001 (2009).
  - <sup>11</sup> T. Kariyado, and M. Ogata, J. Phys. Soc. Jpn. **79**, 083704 (2010).
  - <sup>12</sup> Y. Bang, H. Y. Choi, and H. Won, Phys. Rev. B **79**, 054529 (2009).
  - <sup>13</sup> A. F. Kemper, C. Cao, P. J. Hirschfeld, and H. P. Cheng, Phys. Rev. B **80**, 104511 (2009).
  - <sup>14</sup> K. Nakamura, R. Arita, and H. Ikeda, Phys. Rev. B **83**, 144512 (2011).
  - <sup>15</sup> W. F. Tsai, Y. Y. Zhang, C. Fang, and J. P. Hu, Phys. Rev. B **80**, 064513 (2009).
  - <sup>16</sup> L. Wray, D. Qian, D. Hsieh, Y. Xia, L. Li, J. G. Checkelsky, A. Pasupathy, K. K. Gomes, C. V. Parker, A. V. Fedorov, G. F. Chen, J. L. Luo, A. Yazdani, N. P. Ong, N. L. Wang, and M. Z. Hasan, Phys. Rev. B **78**, 184508 (2009).
  - <sup>17</sup> L. Shan, Y. L. Wang, B. Shen, B. Zeng, Y. Huang, A. Li, D. Wang, H. Yang, C. Ren, Q. H. Wang, S. H. Pan, and H. H. Wen, Nature Physics **4**, 325 (2011).
  - <sup>18</sup> F. Massee, S. de Jong, Y. Huang, J. Kaas, E. van Heumen, J. B. Goedkoop, and M. S. Golden, Phys. Rev. B **80**, 140507(R) (2009).
  - <sup>19</sup> J. E. Hoffman, Rep. Prog. Phys. **74**, 124513 (2011).
  - <sup>20</sup> T. M. Chuang, M. P. Allan, J. Lee, Y. Xie, N. Ni, S. L. Bud'ko, G. S. Boebinger, P. C. Canfield, and J. C. Davis, Science **327**, 181 (2010).
  - <sup>21</sup> G. F. Chen, Z. Li, G. Li, W. Z. Hu, J. Dong, J. Zhou, X. D. Zhang, P. Zheng, N. L. Wang, and J. L. Luo, Chin. Phys. Lett. **25**, 3403 (2008).
  - <sup>22</sup> T. Hanke, S. Sykora, R. Schlegel, D. Baumann, L. Harnagea, S. Wurmehl, M. Daghofer, B. Buchner, J. van den Brink, and C. Hess, Phys. Rev. Lett. **108**, 127001 (2012).
  - <sup>23</sup> S. C. Erwin, and I. I. Mazin, unpublished.
  - <sup>24</sup> Y. Yin, M. Zech, T. L. Williams, X. F. Wang, G. Wu, X. H. Chen, and J. E. Hoffman, Phys. Rev. Lett. **102**, 097002 (2009).
  - <sup>25</sup> F. Massee, Y. Huang, R. Huisman, S. de Jong, J. B. Goedkoop, and M. S. Golden, Phys. Rev. B **79**, 220517 (R) (2009).
  - <sup>26</sup> M. L. Teague, G. K. Drayna, G. P. Lockhart, P. Cheng, B. Shen, H. H. Wen, and N. C. Yeh, Phys. Rev. Lett. **106**, 087004 (2011).
  - <sup>27</sup> Z. H. Liu, P. Richard, K. Nakayama, G. F. Chen, S. Dong, J. B. He, D. M. Wang, T. L. Xia, K. Umezawa, T. Kawahara, S. Souma, T. Sato, T. Takahashi, T. Qian, Yaobo Huang, Nan Xu, Yingbo Shi, H. Ding, and S. C. Wang, Phys. Rev. B **84**, 064519 (2011).
  - <sup>28</sup> R. C. Dynes, J. P. Garno, G. B. Hertel, and T. P. Orlando, Phys. Rev. Lett. **53**, 2437 (1984).
  - <sup>29</sup> T. Kariyado, and M. Ogata, J. Phys. Soc. Jpn. **79**, 033703 (2010).
  - <sup>30</sup> A. Weie, G. Wellein, A. Alvermann, and H. Fehske, Rev. Mod. Phys. **78**, 275 (2006).
  - <sup>31</sup> L. Fang, H. Q. Luo, P. Cheng, Z. S. Wang, Y. Jia, G. Mu, B. Shen, I. I. Mazin, L. Shan, C. Ren, and H. H. Wen, Phys. Rev. B **80**, 140508(R) (2009).
  - <sup>32</sup> H. Wadati, I. Elfimov, and G. A. Sawatzky, Phys. Rev. Lett. **105**, 157004 (2010).
  - <sup>33</sup> G. Levy, R. Sutarto, D. Chevrier, T. Regier, R. Blyth, J. Geck, S. Wurmehl, L. Harnagea, H. Wadati, T. Mizokawa, I. S. Elfimov, A. Damascelli, and G. A. Sawatzky, Phys. Rev. Lett. **109**, 077001 (2012).
  - <sup>34</sup> Q. M. Si, and E. Abrahams, Phys. Rev. Lett. **101**, 076401 (2008).
  - <sup>35</sup> K. Seo, B. A. Bernevig, and J. P. Hu, Phys. Rev. Lett. **101**, 206404 (2008).